Donor–π-Acceptor Species Derived from Functionalised 1,3-Dithiol-2-ylidene Anthracene Donor Units Exhibiting Photoinduced Electron Transfer Properties: Spectroscopic, Electrochemical, X-Ray Crystallographic and Theoretical Studies

Andrei S. Batsanov, Martin R. Bryce,* Malcolm A. Coffin, Andrew Green, Ronald E. Hester,* Judith A. K. Howard, Igor K. Lednev, Nazario Martín,* Adrian J. Moore, John N. Moore,* Enrique Ortí,* Luis Sánchez, María Savirón, Pedro M. Viruela, Rafael Viruela, and Tian-Qing Ye

Abstract: Novel single-component donor–acceptor species **7** and **8** have been synthesised from substituted 10-(1,3-dithiol-2-ylidene)anthracen-9(10H)one **6** by reaction with Lehnert's reagent and with *N*,*N*′-bis(trimethylsilyl)carbodiimide, respectively. The steady-state UV/visible spectra of these systems contain a solvatochromic band arising from intramolecular charge transfer between the donor and acceptor groups. Ultrafast time-resolved spectroscopy shows that the excited state formed on photolysis has a lifetime of 170–400 ps, which depends strongly on solvent polarity. Cyclic voltammetric data indicate the presence of two active redox centres in the molecules: electrochemical oxidation and reduction form cation radicals and anion radicals, respectively. The X-ray crystal structures of compounds **6a**, **7b** and **11a** reveal that all three molecules are severely distorted from planarity, with the central ring of the anthracenediylidene moiety adopting a boat conformation. The molecular structures of **6**, **7**, and **11** have been investigated theoretically at the ab initio 6–31G* level. Calculated geometries are in good agreement with the X-ray data and clearly show the decrease in steric hindrance along the series **11** > **7** > **8** > **6**. The calculations support the intramolecular charge-transfer nature of the lowest energy absorption band observed for **6**, **7** and **8**, and explain the origin of the redox properties for these compounds. The optimised geometries of the cation radical, anion radical and dianion of compound **7** illustrate the structural changes induced by the charging process. For the dianion, the steric interactions are alleviated by rotation of the acceptor dicyanomethylene unit, but the presence of the donor dithiole group hinders the achievement of a fully aromatic planar structure for the central anthracene skeleton.

Keywords: ab initio calculations · crystal structures · cyclic voltammetry · 1,3-dithioles · electron transfer

Introduction

The synthesis of organic molecules with delocalised π electron systems bearing both electron-donor and electron-acceptor moieties within the same molecule has received much attention, due to the interesting unconventional optoelectronic properties they exhibit. These systems are currently being explored within the wide fields of nonlinear optics,[1] molecular electronics,[2] artificial photosynthetic models[3] and solvatochromic effects.[4] They are also of great interest in the field of physical organic chemistry.[5] Recently, we reported the synthesis of donor–π-acceptor compounds based on the acceptor 7,7,8,8-tetracyano-*p*-quinodimethane (TCNQ), which exhibit photoinduced charge-transfer properties.[6] We have also studied the effect of varying the conjugated spacer unit within the TCNQ[7] and the tetrathiafulvalene (TTF)[8] frameworks.

Organic compounds of the push-pull type containing a quinonoid ring connecting both donor and acceptor moieties are particularly interesting, since the push-pull stabilisation is promoted by the aromatisation of the benzoquinonoid ring. Thus, the benzoquinonoid compound **1** and its benzo-fused derivatives were reported by Gompper et al. thirty years ago as highly coloured chromophores, showing a strong absorp-

[*] Prof. M. R. Bryce, Dr. A. Green, Dr. A. J. Moore, Dr. M. A. Coffin, Dr. M. Savirón, Dr. A. S. Batsanov, Prof. J. A. K. Howard
Department of Chemistry, University of Durham
South Road, Durham, DH1 3LE (UK)
Prof. Dr. N. Martín,* Dr. L. Sánchez
Departamento de Química Orgánica, Facultad de Química, Universidad Complutense
E-28040 Madrid (Spain)
Prof. Dr. E. Ortí, Prof. Dr. P. M. Viruela, Prof. Dr. R. Viruela
Departamento de Química Física, Universidad de Valencia
E-46100 Burjassot, Valencia (Spain)
Prof. R. E. Hester, Dr. J. N. Moore, Dr. I. K. Lednev, Dr. T.-Q. Ye
Department of Chemistry, University of York
Heslington, York, YO1 5DD (UK)

  0947-6539/98/0412-2580 $ 17.50+.50/0

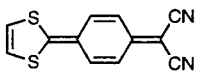

1

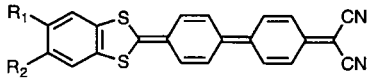

2 $R_1 = R_2 = H$
$R_1 = H, R_2 = Me$

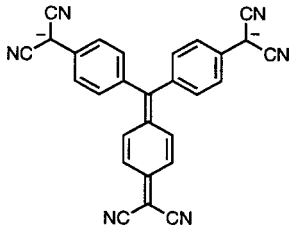

3

Abstract in Spanish: *Los nuevos compuestos dador–aceptor **7** y **8** se han sintetizado a partir de 10-(1,3-ditiol-2-iliden)-antracen-9(10H)-onas **6** diferentemente sustituídas utilizando el reactivo de Lehnert y N,N′-bis(trimetilsilil)carbodiimida, respectivamente. Los espectros UV/visible de estado estacionario de estos sistemas muestran una banda solvatocrómica que implica un proceso de transferencia de carga intramolecular desde el fragmento dador al aceptor. La espectroscopía ultrarápida a tiempo resuelto revela que el estado excitado obtenido por fotólisis de estos compuestos tiene un tiempo de vida media de 170–400 ps; el cual presenta una acusada dependencia respecto a la polaridad del disolvente. Los datos de voltamperometría cíclica confirman la existencia de dos centros redox activos en este tipo de moléculas: la oxidación y la reducción electroquímica forman los respectivos catión radical y anión radical. Las estructuras cristalinas de rayos-X de los compuestos **6a**, **7b** y **11a** revelan que dichas moléculas están fuertemente distorsionadas de la planaridad con el anillo central de antracenodiilideno en una conformación de bote. La estructura molecular de los compuestos **6**, **7** y **11** también ha sido investigada mediante cálculos teóricos a nivel ab initio 6–31G*. Las geometrías calculadas coinciden bastante bien con las obtenidas mediente difracción de rayos-X e indican claramente una disminución de la repulsión estérica de acuerdo con la siguiente serie: **11** > **7** > **8** > **6**. Los cálculos teóricos confirman la naturaleza de la transferencia de carga intramolecular de la banda de baja energía observada en los espectros UV/visible de los compuestos **6**, **7** y **8** y explican los valores de los potenciales redox determinados mediante voltamperometría cíclica. Las geometrías optimizadas para el catión radical, anión radical y dianión del compuesto **7** ilustran los cambios estructurales provocados por el proceso de adquisición de carga. En el caso del dianión, las interacciones estéricas disminuyen notablemente como consecuencia de la rotación de la subunidad aceptora de dicianovinileno, aunque la presencia del fragmento dador impide la formación de una estructura aromática completamente plana del esqueleto central de antraceno.*

tion band in the visible region.[9] The push-pull diphenoquinonoid compounds **2,** bearing a benzo-1,3-dithiol-2-ylidine unit as a strong donor group and a dicyanomethylene unit as a strong acceptor moiety, have been recently synthesised and show a strong absorption band in the near infrared region.[10] The observed large negative solvatochromism with increasing solvent polarity indicates that zwitterionic forms contribute greatly to the push-pull quinonoid system in compound **2**.

The hexacyanotriquinarenemethane dianion **3** bearing the dicyanomethylene unit covalently attached to the quinonoid ring has been recently reported as a stable, highly tetrapolar substance, which behaves as a donor–acceptor system.[11]

In this paper, we report the synthesis, steady-state and ultrafast time-resolved UV/visible spectroscopy, solution electrochemistry and molecular structure (determined by X-ray structural analyses and/or by ab initio calculations) of donor–π-acceptor systems which are based upon the 9,10-anthracenediylidene core.[12] The donor units are 1,3-dithiole rings and the acceptor units are ketone, dicyanomethylene and *N*-cyanoimine groups. The donor ability can be finely tuned by the attachment of different substituents to the 1,3-dithiole rings.

Results and Discussion

Synthesis: The ketones **6** required for the synthesis of systems **7** and **8** were readily prepared by reaction of the corresponding 1,3-dithiolium cation salt **4a–d** (Scheme 1) with anthrone **5**. This was carried out in the presence of sodium ethoxide in the case of **4a**, or pyridine/acetic acid for **4b–d**, following literature precedents.[13] Compounds **7a–d** were subsequently prepared in good to excellent yields (54–84%) by the reaction of **6a–d** with Lehnert's reagent (malononitrile, pyridine and titanium tetrachloride)[14] in refluxing chloroform. Similarly, the reaction of **6a–d** with *N,N*-bis(trimethylsilyl)carbodiimide (BTC) and titanium tetrachloride, following the conditions developed by Aumüller and Hünig for the synthesis of *N,N′*-dicyanoquinone diimine acceptors,[15] resulted in the formation of the *N*-cyanoimine donor–π-acceptor systems **8a–d** (23–85% yields). These cyanoimination reactions required notably longer reaction times (typically 2–3 days) than the corresponding dicyanomethylations (1 day) and the addition of further BTC during the reaction was found to improve the yield of products **8**. The ^{1}H NMR spectra of **8** at room temperature exhibited very broad peaks in the aromatic region. By performing variable-temperature NMR studies, we were able to produce significantly better resolved spectra (temperatures below $-30\,^\circ$C produced sharp peaks; Figure 1). This broadness at $> -30\,^\circ$C is attributed to the cyanoimine group flipping on the NMR timescale, causing the *peri* hydrogen signals to broaden, thereby affecting the rest of the aromatic region of the spectra. Similarly, the ^{13}C NMR spectra also showed broad peaks around $\delta = 126$, due to the two *peri* carbon atoms.

We have also synthesised the new 9,10-bis(1,3-dithiol-2-ylidene)-9,10-dihydroanthracene derivative **11a** (Scheme 2) for a comparison of the X-ray structure with compounds **6a**

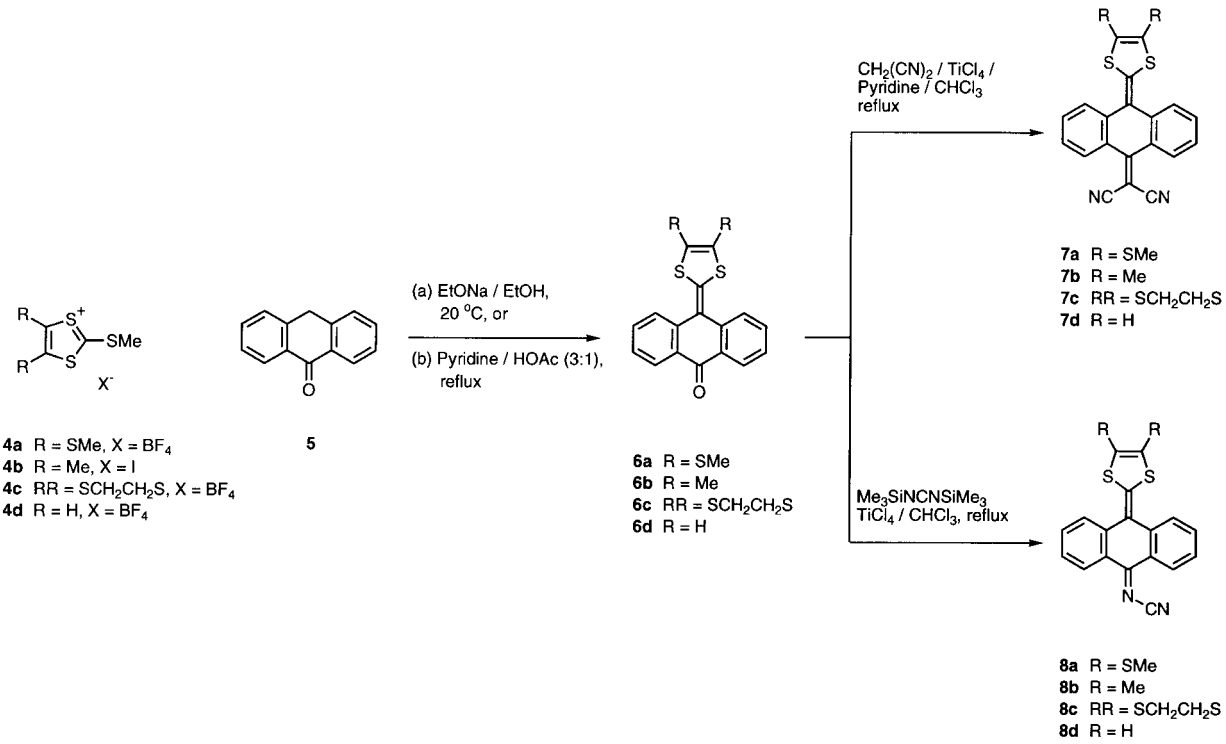

Scheme 1. Synthesis of compounds **6a–d**, **7a–d** and **8a–d**.

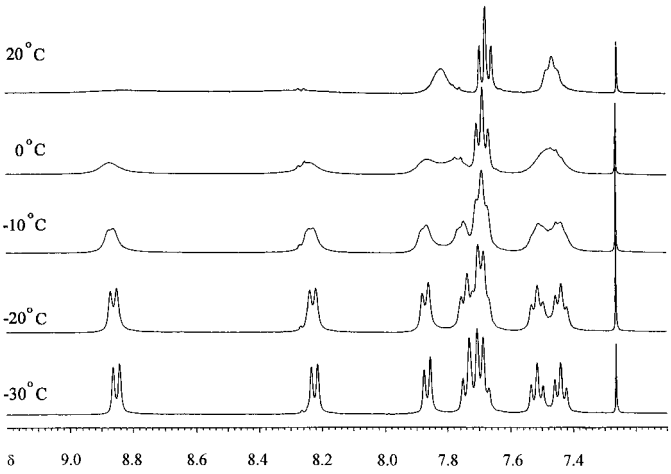

Figure 1. Variable temperature ^{1}H NMR spectra of compound **8a**.

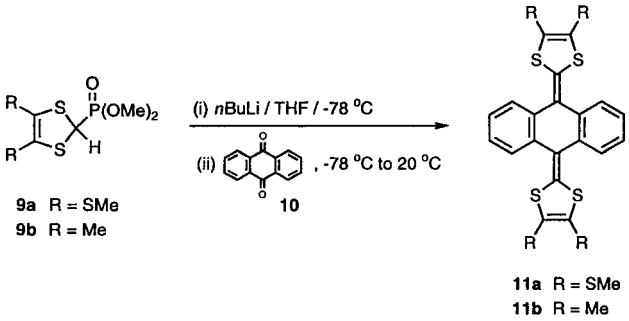

Scheme 2. Synthesis of compounds **11a,b**.

and **7b**. Twofold reaction of anthraquinone **10** with the carbanion generated from phosphonate reagent **9a**[16] (*n*BuLi at −78 °C in THF) afforded compound **11a** in 38% yield.

Steady-state UV/visible absorption and emission spectroscopy: The electronic absorption and emission spectra of compounds **7**, **8** and **11b**[8b] in solution have been recorded for several different solvents, as illustrated in Figure 2 for **7b** and in Figure 3 for **11b**. The absorption profiles of the donor–

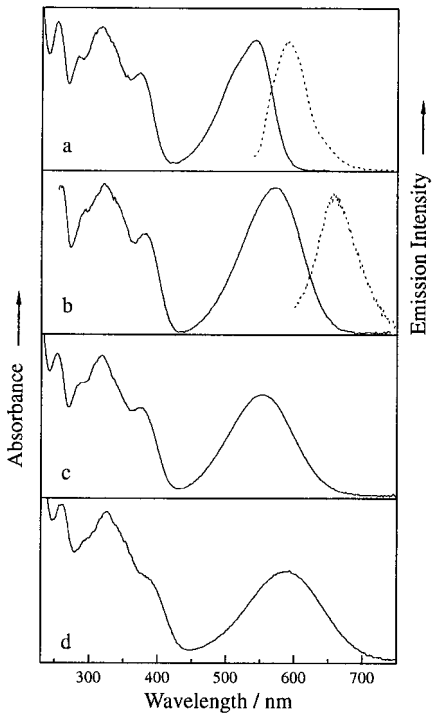

Figure 2. Normalised UV/visible absorption (solid line) and emission (dashed line) spectra of **7b** in a) cyclohexane, b) chloroform, c) acetonitrile and d) aqueous solution.

0947-6539/98/0412-2582 $ 17.50+.50/0 *Chem. Eur. J.* **1998**, *4*, No. 12

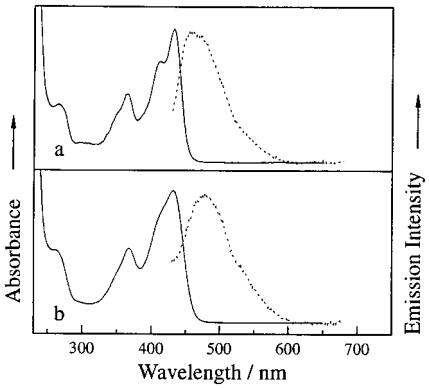

Figure 3. Normalised UV/visible absorption (solid line) and emission (dashed line) spectra of **11b** in a) cyclohexane and b) acetonitrile solution.

acceptor compounds **7** and **8** are similar, comprising a set of peaks in the UV region at wavelengths < 450 nm and a broad, low-energy band in the visible region at 550–600 nm. This visible wavelength band may be assigned to an intramolecular charge-transfer transition from the donor 1,3-dithiole moiety to the acceptor group, similar to those observed in other single component donor–π-acceptor systems.[6] The charge-transfer bands of compounds **8** are shifted hypsochromically from those of compounds **7** (Table 1), this shift being attributable to the electron-accepting ability of the N–CN group being less than that of the $C(CN)_2$ group.[15] The precursor ketones **6** show charge-transfer bands shifted to shorter wavelengths (460–480 nm), owing to the poorer acceptor ability of the ketone group. The charge-transfer band position is also sensitive to variation of the subtituents on the 1,3-dithiole ring (Table 1), with that of **7b** being shifted bathochromically from those of **7a**, **7c** and **7d**, due to the increased electron-donating ability of the dimethyl 1,3-dithiol group of **7b**. The absorption spectrum of the symmetric bis(1,3-dithiole) derivative **11b** (Figure 3) is clearly different from those of compounds **7** and **8**; it comprises only UV bands and no low-energy band in the visible region. The absence of a charge-transfer band for **11b** is expected due to the lack of an acceptor group within this molecule.

Compound **7b** was found to exhibit solvatochromism, as illustrated in Figure 2 and detailed in Table 2. The UV absorption bands of **7b** show little dependence on solvent, whereas the charge-transfer band exhibits a bathochromic shift and an increase in bandwidth with increasing solvent polarity, although the peak positions for chloroform and acetonitrile are reversed from this general trend. The emission from **7b** was also found to be dependent on solvent, being weak in cyclohexane, very weak in chloroform and unobserved in acetonitrile or aqueous solutions. The emission band exhibits both a bathochromic shift and a larger Stokes shift from the absorption band on increasing the solvent polarity (from cyclohexane to chloroform), although the bandwidths are similar. In contrast, both the absorption and the very weak emission of **11b** were found to be insensitive to changes of solvent (Figure 3), as expected in the absence of a charge-transfer transition.

Table 2. UV/visible charge-transfer absorption band maxima (λ_{abs}) and widths[a] ($\Delta\lambda_{abs}$), and emission band maxima (λ_{em}), intensities,[b] widths ($\Delta\lambda_{em}$) and Stokes shifts ($\Delta\lambda_{Stokes}$) for **7b** in solution, along with solvent dielectric constants (ε) at 30 °C.

Solvent	ε	λ_{abs} [nm]	λ_{abs} [nm]	$\Delta\lambda_{em}$ [nm]	$\Delta\lambda_{em}$ [nm]	$\Delta\lambda_{Stokes}$ [nm]
cyclohexane	2.02	542	81	590 (w)	61	48
chloroform	4.80	571	102	658 (vw)	66	87
acetonitrile	37.5	553	111	-	-	-
water	77.0	592	128	-	-	-

[a] Full width at half maximum; [b] w = weak, vw = very weak, - = unobserved.

Table 1. Electronic absorption maxima[a] and redox potentials[b] of compounds **6**–**8**.

	Compound	λ_{max} [nm]	E^1_{ox} [V]	E^1_{red} [V]
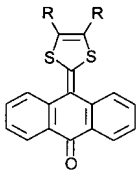	**6a:** R = SMe	455	0.98	–1.45
	6b: R = Me	481	0.87	–1.52
	6c: R = $(SCH_2)_2$	460	0.95	–1.47
	6d: R = H	467	0.96	–1.52
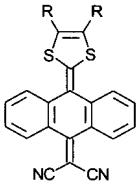	**7a:** R = SMe	545	0.98	–1.00
	7b: R = Me	572	0.95	–0.96
	7c: R = $(SCH_2)_2$	550	0.99	–0.97
	7d: R = H	542	1.05	–1.04
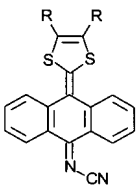	**8a:** R = SMe	542	0.97	–1.04
	8b: R = Me	566	0.85	–1.08
	8c: R = $(SCH_2)_2$	558	0.97	–1.01
	8d: R = H	543	0.89	–1.00

[a] In CH_2Cl_2 solution, 20 °C [b] Potentials vs. SCE; $Bu_4N^+ClO_4^-$ 0.1M as supporting electrolyte; GCE as working electrode; CH_2Cl_2 as solvent; scan rate: 200 mV s^{-1}; 20 °C.

Ultrafast time-resolved UV/visible spectroscopy: The photophysics of **7b** has been studied by ultrafast time-resolved UV/visible spectroscopy. The time-resolved difference spectra, obtained 4–5 ps after photolysis, are illustrated in Figure 4 for **7b** in acetonitrile and in chloroform on UV (303 nm) or visible (606 nm) excitation. These time-resolved difference spectra have similar profiles, comprising photoinduced absorption at 400–580 nm and a negative feature at approximately 750 nm. The kinetics of the transient signals obtained on UV photolysis of **7b** in acetonitrile (shown in Figure 5 for probe wavelengths of 500 and 800 nm) were found to fit well to a single-exponential decay corresponding to a lifetime ($\tau_{obs} = 1/k_{obs}$) of 170 ± 20 ps. Similar kinetics were obtained on visible-wavelength photolysis. The

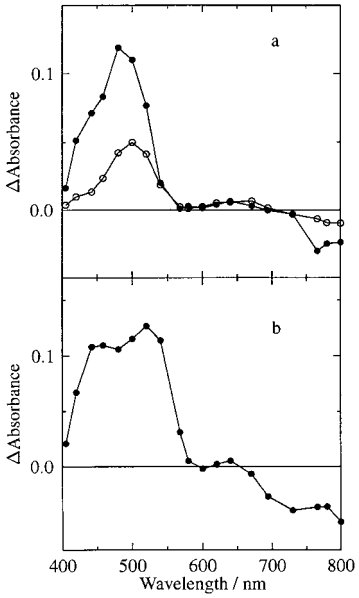

Figure 4. Time-resolved UV/visible difference spectra of **7b** in acetonitrile at 4 ps (top) and in chloroform at 5 ps (bottom), after photolysis at 606 nm (●) or 303 nm (○).

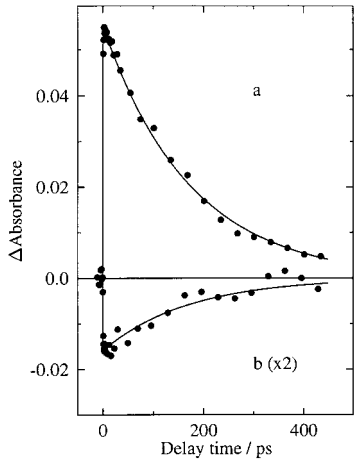

Figure 5. Transient kinetic signals at a) 500 nm and b) 800 nm (expanded by × 2), obtained on 303 nm photolysis of **7b** in acetonitrile. The data (●) are fitted (solid line) by a single-exponential decay function corresponding to a lifetime of 170 ps.

excited state lifetime was found to be extended considerably for **7b** in chloroform, preliminary experiments giving $\tau_{obs} \approx$ 400 ps.

The similar transient spectra and kinetics obtained on either UV or visible excitation indicate that internal conversion occurs rapidly from the higher excited states formed initially on UV photolysis. The same excited state is observed here on either UV or visible excitation. The strong positive feature at approximately 500 nm in the transient difference spectra is attributable to absorption of the excited state. The absence of a negative feature at 500 – 650 nm, which would be expected from bleaching of the ground state absorption band, indicates that the excited state also absorbs in this region and that the profile is the result of contributions from both ground and excited states. The negative feature observed at wavelengths > 650 nm for **7b** in chloroform, and at > 720 nm for **7b** in acetonitrile, may be attributed to excited state emission which is stimulated by the probe pulse; spontaneous (non-stimulated) emission would be observed in these experiments as an increase in probe beam intensity which is independent of delay time. It is notable that the stimulated emission band of **7b** in chloroform (Figure 4 bottom) does not match the steady-state emission band (Figure 2b), which peaks at 658 nm and shows essentially no emission around 800 nm. The stimulated emission of **7b** in acetonitrile appears to be shifted to longer wavelength than that in chloroform, consistent with the expected dependence on solvent polarity. No steady-state emission was observed for **7b** in acetonitrile to enable comparison.

The observation of emission bands at different wavelengths in steady-state and time-resolved experiments suggests two possibilities. First, that the same emission bands are observed in each experiment, but that the emission profile observed in the time-resolved experiments is distorted by the presence of a strong, overlying transient absorption band from the excited state. Second, that at least two excited states form on excitation of **7b** in solution, and that the steady-state and time-resolved experiments probe the emission from different states. The considerable difference in the emission bands observed in these two sets of experiments suggests that the second possibility is the more likely. Moreover, the phenomenon of dual emission has been observed in a number of cases involving charge-transfer excitation within organic donor – acceptor systems,[17] arising from the general photophysical mechanism given in Scheme 3. The ground state (S_0) is promoted to an excited state (S_1), which may decay back to the ground state radiatively (k_r^1) or nonradiatively (k_{nr}^1), or it may relax (k^1) to a more stable form ($S^\dagger$), which may also decay by radiative ($k_r^\dagger$) or nonradiative ($k_{nr}^\dagger$) pathways; the ground state ultimately is reformed. The $S^\dagger$ state is formed in higher yield in solvents of high polarity and it exhibits emission that is at lower energy than that of the first formed S_1 state. The nature of the $S^\dagger$ species has generally been described as a twisted intramolecular charge-transfer (TICT) state,[17–19] although this interpretation has been disputed and $S^\dagger$ has been described alternatively as a solute/solvent exciplex.[20] The observations reported here for **7b** are in accord with the general mechanism given in Scheme 3, whatever the precise nature of the $S^\dagger$ state.

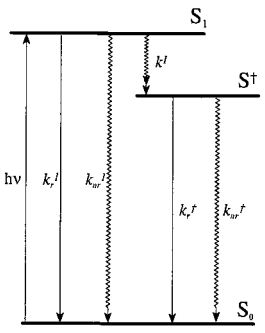

Scheme 3. General photophysical mechanism for **7b**.

The emission observed from **7b** in steady-state experiments mirrors the charge-transfer absorption band and may be attributed to the S_1 state. The emission band position shifts to longer wavelengths and there is a larger Stokes shift with increasing solvent polarity, because more polar solvents enable the first formed charge-transfer state to be stabilised more effectively. According to this scheme, increased solvent polarity will increase k^1, increase the yield of $S^\dagger$ and hence decrease the yield of emission from S_1; this trend of weaker

  0947-6539/98/0412-2584 $ 17.50+.50/0 *Chem. Eur. J.* **1998**, *4*, No. 12

emission with increasing solvent polarity is observed for **7b**. The stimulated emission, observed at longer wavelength in the time-resolved experiments, may be attributed to the $S^{\dagger}$ state; the risetime of this signal at 800 nm is very short (<5 ps) in acetonitrile, corresponding to the timescale of the $S_1 \rightarrow S^{\dagger}$ reaction and/or solvent stabilisation of the $S^{\dagger}$ state. Whether this reaction is complete, or whether equilibrium is established between the S_1 and $S^{\dagger}$ excited states, is unclear from the present data and may depend on the solvent environment, which determines the relative energies of these states. Thus, the observed transient spectra may contain contributions from both of these states; the observed lifetimes correspond to the overall timescale for excited state decay and ground state recovery.

In summary, these preliminary ultrafast spectroscopic studies indicate that at least two excited states may contribute to the photophysics of **7b** and that the excited state lifetime depends strongly on solvent polarity. The observations are consistent with the general schemes reported for related donor–acceptor excited states. More extensive studies of the excited-state structure and dynamics will be required to establish more detailed aspects of the photophysical mechanism.

Solution electrochemistry: The solution electrochemistry of compounds **6–8** has been studied by cyclic voltammetry. Systems **6–8** exhibit a reversible oxidation wave that can be attributed to the formation of the radical cation of the 1,3-dithiole donor moiety. The half-wave potentials recorded for these systems (Table 1) reveal that they are poor donors compared to the parent TTF ($E^1_{ox} = 0.35$ V, under the same conditions). Their donor ability is, however, better than that of perylene ($E^1_{ox} = 1.03$ V versus SCE)[21] and many other organic donor systems, such as dioxins ($E^1_{ox} = 1.0-1.2$ V versus SCE).[22] Derivatives **6b**, **7b** and **8b** show lower oxidation potentials, owing to the electron-donating effect of the two attached methyl groups. This effect is consistent with the longer wavelengths observed for the charge-transfer bands of the methyl-substituted compounds (see Table 1).

The voltammograms of compounds **6–8** (exemplified in Figure 6 for **6d** and **7d**) also show a reduction wave on forming the corresponding radical anion, for which the negative charge is presumably located on the acceptor group, as has been proved for TCNQ derivatives.[23] A second, poorly defined reduction wave is observed in all cases at more negative potentials, whose assignment is discussed below on the basis of ab initio calculations. The first reduction potential of the precursor ketones **6** is cathodically shifted by approximately 0.5 V compared to **7** and **8**, owing to the lower acceptor ability of the ketone group. This is in agreement with the shorter wavelength observed for the charge-transfer band (see Table 1).

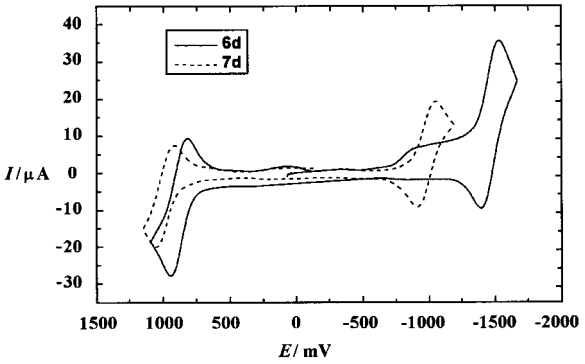

Figure 6. Cyclic voltammograms of compounds **6d** and **7d** at 200 mV s^{-1} in dichloromethane.

X-ray crystal structures analysis of 6a, 7b and 11a: Compounds **6a**, **7b** and **11a** were characterised by single-crystal X-ray diffraction (Table 3). The asymmetric unit of **7b** comprises two molecules with essentially the same geometry. In **11a**, one of the methyl groups is disordered over two positions. All three molecular structures (Figure 7) are distorted significantly from planarity, similar to compounds **11b**,[8b] **12** and the radical cation of the latter[24] and have noncrystallographic mirror symmetry. The central (quinone) ring of the anthraquinone moiety adopts a boat conformation (somewhat twisted in structure **6a**), while the two outer benzene rings are tilted in the opposite direction and form a dihedral angle

Table 3. Crystal data for compounds **6a**, **7b** and **11a**.

Compound	**7b**	**6a**	**11a**
formula	$C_{22}H_{14}N_2S_2$	$C_{19}H_{14}OS_4$	$C_{24}H_{20}S_8$
M	370.5	386.5	564.9
T[K]	150	293	293
symmetry	monoclinic	monoclinic	triclinic
a [Å]	15.353(5)	11.703(2)	8.771(1)
b [Å]	13.895(5)	8.255(2)	9.993(1)
c [Å]	17.082(6)	18.300(4)	15.375(1)
α [°]	90	90	86.93(1)
β [°]	101.07(3)	97.15(3)	78.69(1)
γ [°]	90	90	75.24(1)
U [Å^3]	3576(2)	1755.1(8)	1277.8(3)
reflections/lattice	500	25	25
θ range [°]	4–23	10–15	12–15
space group	$P2_1/n$	$P2_1/n$	$P\bar{1}$
Z	8	4	2
F(000)	1536	800	584
μ(MoK_α) [cm^{-1}]	3.1	5.4	7.1
ρ_{calcd} [g cm^{-3}]	1.38	1.46	1.47
crystal size [mm]	$0.08 \times 0.25 \times 0.5$	$0.07 \times 0.45 \times 0.5$	$0.2 \times 0.2 \times 0.4$
scan mode	ω	$\theta/2\theta$	$\theta/2\theta$
$2\theta_{max}$ [°]	46.5	55	54
data total	13194	4497	5289
data unique	5101	4024	4996
data observed $I > 2\sigma(I)$*	4610	2999	3056
R_{int}	0.030	0.015	0.023
absorption corr.	-	empirical	empirical
ψ scans (reflections)	-	216 (6)	144 (3)
T_{min}:T_{max}	-	0.839:1	0.920:1
no. of variables	477	273	300
wR, all data	0.094	0.045	0.054
goodness-of-fit	1.16	1.52	1.54
R(F), obs. data	0.041	0.037	0.041
$\Delta\rho_{max}$ [e Å^{-3}]	0.17	0.30	0.38
$\Delta\rho_{min}$ [e Å^{-3}]	−0.21	−0.22	−0.41

[*] $F^2 > 2\sigma(F^2)$

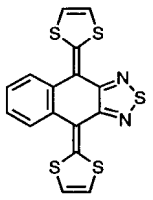

12

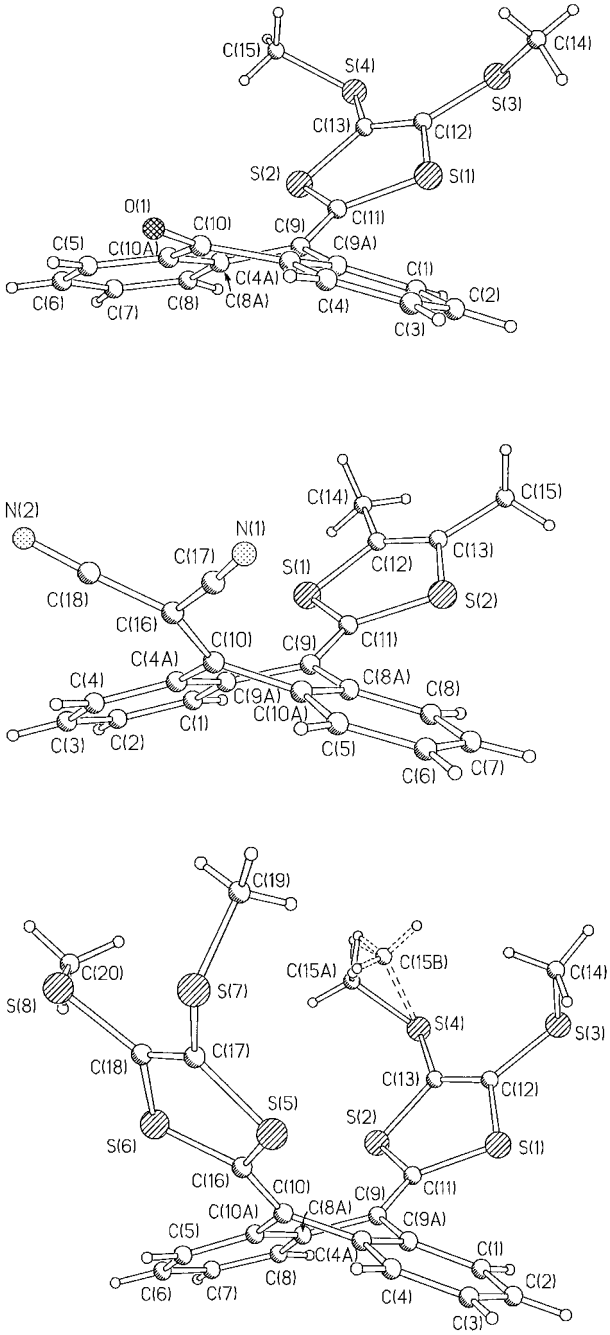

Figure 7. Molecular structures of **6a** (top), **7b** (centre) and **11a** (bottom, showing the disorder of the SMe group).

of 27° (**6a**), 35 or 32° (**7b**) and 38° (**11a**). There is also tilting of the exocyclic C(9)=C(11) and C(10)=C(16) bonds out of the planes of the adjacent ring moieties (by 3–5°) or the $C(CN)_2$ moiety in **7b** (by approximately 10°) and folding of the dithiole rings along the S–S vectors (by 8–12°) in all three structures in the same ('inward') direction. Such a conformation is apparently forced by steric repulsion between the dithiole ring sulfur atoms and the *peri*-hydrogen atoms. These S–H contacts in **6a**, **7b** and **11a** (2.5–2.6 Å) are substantially shorter than the sum of the Van der Waals radii of H (1.17 Å) and S (1.8 Å),[25] while in an (imaginary) planar structure they should be forbiddingly short (approximately 2 Å). Indeed, replacement of a less bulky substituent for one dithiolylidene group reduces the bending of the molecules **6a** and **7b**. In their structures, folding of the central ring is much smaller along the C(4a)–C(10a) vector than along the C(8a)–C(9a) vector, that is 14° versus 26° in **6a**, 23° versus 29° in **7b**, while in bis(dithiole) compounds the folding is larger and symmetrical (31° in both **11a** and **11b**[8b]), in direct proportion to the size of the substituent. Furthermore, similar molecules where the peripheral benzene rings are absent, as in bis(4,5-dimethyl-1,3-dithiol-2-ylidene)-1,4-cyclohexa-2,5-diene,[26] or replaced by 1,2,5-thiadiazole[27] or 1,4-diazine[28] rings, are essentially planar and form infinite stacks in the crystal (in the last two compounds, attractive intramolecular S···N contacts replace the repulsive S···H contacts in **11a**). The distorted conformations of **6a**, **7b** and **11a** preclude efficient stacking in the crystal. Instead, the inversion-related molecules 'engulf' each other (Figure 8) at the usual Van der Waals distances.

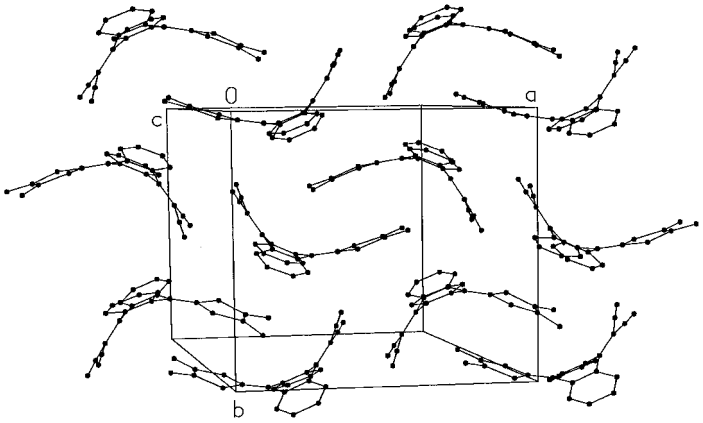

Figure 8. Crystal packing of **7b**.

Ab initio calculations

Neutral compounds: The molecular structures of the unsubstituted compounds **6d**, **7d**, **8d** and **11d** (R = H) were optimised at the ab initio 6–31G* Hartree–Fock (HF) level in both planar and nonplanar conformations. The planar structures are strongly hindered by the very short contacts between the sulfur atoms and the hydrogen atoms in *peri* positions, which are calculated to be 2.13 (**6d**), 2.05 (**7d**), 2.10 (**8d**) and 2.02 Å (**11d**). Compared to **11d**, the $S{-}H_{peri}$ contacts on one side of **7d** are substituted by two $C{-}H_{peri}$ (1.96 Å) and two $N{-}H_{peri}$ (2.29 Å) contacts. The greater flexibility of the cyanoimine group in **8d** relaxes the unique $C{-}H_{peri}$ and $N{-}H_{peri}$ contacts to 2.12 and 2.43 Å, respectively. Compound **6d** exhibits no significant steric hindrance on the acceptor part. These interactions determine that all four compounds distort from planarity and adopt the butterfly-shaped conformations depicted in Figure 7, where the central quinone ring shows a boat conformation and the lateral benzene rings preserve their planarity. 6–31G* calculations predict that the energy difference between planar and butterfly structures increases along the series **6d** (18.02 kcal mol^{-1}) < **8d** (24.15 kcal mol^{-1}) < **7d** (43.55 kcal mol^{-1}) < **11d** (57.44 kcal mol^{-1}), in accord with the steric hindrance and justifying the more folded structures found along this series. The outer benzene rings form a dihedral angle of 29.6° (**6d**),

0947-6539/98/0412-2586 $ 17.50+.50/0 *Chem. Eur. J.* **1998**, *4*, No. 12

35.9° (**8d**), 41.8° (**7d**) and 43.7° (**11d**), and the central ring is bent along the C(4a)–C(10a) and C(8a)–C(9a) vectors by 17.3° and 31.6° (**6d**), 26.3° and 33.5° (**8d**), 34.6° and 35.4° (**7d**) and 36.6° (**11d**). These values follow the same trends established from X-ray data for **6a**, **7b** and **11a**. These values are slightly larger than those measured experimentally, since ab initio calculations are performed on isolated molecules and packing forces in the crystal tend to flatten the molecules to achieve the most compact packing.

Table 4 summarises the bond lengths calculated for the central dithiole–quinonoid–dicyanomethylene skeleton of **7d**, which are compared with those obtained for **7b** from X-ray data and only marginally exceed the 3σ values of the experiment. The average deviation between the theoretical and the experimental values is 0.017 Å. The largest deviations correspond to the C(9)–C(11) and C(10)–C(16) double bonds, which are calculated approximately 0.025 Å too short, and to the S(1),S(2)–C(11) bonds, which are predicted too long by 0.027 Å. Theory predicts and experiments show that the C(4a)–C(9a) and C(8a)–C(10a) bonds of the central quinonoid ring have a length of 1.40–1.41 Å, which is considerably longer than a formal double bond (1.34 Å for ethylene). The lengthening of these bonds is a consequence of the fusion of the outer benzene rings, which have bond lengths of 1.39–1.40 Å and bond angles of 120 ± 1°, thus preserving their aromaticity. The C(9)–C(8a),C(9a) and C(10)–C(4a),C(10a) bonds have lengths of 1.47 Å (1.49 Å from theory) typical of C_{sp^2}–C_{sp^2} single bonds. From the structural standpoint, compounds **7** can be then visualised as two aromatic benzene rings linked together by a 1,3-dithiol-2-ylidene unit and a dicyanoethylidene unit. Similar structural conclusions can be inferred for compounds **6**, **8** and **11**.

Table 4. Selected experimental and calculated bond lengths (in Å).

Bond	**6a**[a]	**7b**[a]	**11a**[a]	**7d**[b]	**7d**$^{+\bullet}$[b]	**7d**$^{-\bullet}$[b]	**7d**$^{2-}$[b]
C(12)–C(13)	1.339(3)	1.331(4)	1.334(7)	1.315	1.330	1.316	1.317
C(12)–S(1)	1.757(2)	1.750(3)	1.759(5)	1.755	1.725	1.757	1.762
S(1)–C(11)	1.763(2)	1.754(3)	1.767(4)	1.781	1.721	1.791	1.796
C(11)–C(9)	1.372(3)	1.374(3)	1.359(6)	1.338	1.404	1.335	1.361
C(9)–C(8a)	1.470(3)	1.470(3)	1.480(6)	1.488	1.473	1.484	1.468
C(8a)–C(10a)	1.417(3)	1.411(3)	1.407(5)	1.403	1.406	1.411	1.431
C(10a)–C(10)	1.481(4)	1.465(3)	-	1.486	1.487	1.466	1.415
C(10)–C(16)	-	1.372(3)	-	1.347	1.342	1.436	1.499
C(16)–C(17)	-	1.439(3)	-	1.443	1.443	1.419	1.407
C(17)–N(1)	-	1.148(3)	-	1.136	1.135	1.145	1.153
C(10)–O(1)	1.230(3)	-	-	-	-	-	-

[a] X-Ray data averaged over chemically equivalent bonds (and over two independent molecules in **7b**) [b] 6–31G* calculations on the most stable butterfly-shaped conformation; all species have a mirror symmetry plane passing through the C(11)–C(9) and C(10)–C(16) bonds (see Figure 11).

Figure 9 indicates the atomic orbital (AO) composition of the highest occupied molecular orbital (HOMO) and lowest unoccupied molecular orbital (LUMO) of **7d**. While the HOMO is mostly sited on the 1,3-dithiol-2-ylidene moiety, the LUMO concentrates on the dicyanoethylidene unit. Similar topologies are found for **6d** and **8d** with the difference that the LUMO of **6d** shows larger contributions from the anthracene moiety. The topologies of the frontier orbitals suggest that, in a first approach, the electron extracted upon oxidation is mainly removed from the 1,3-dithiol-2-ylidene unit and the electron introduced upon reduction is mainly added to the C=O (**6d**), C=C(CN)$_2$ (**7d**) or C=N–CN (**8d**) units, with a large involvement of the anthracene moiety in the case of **6d**. The energy of the LUMO decreases along the series, **6d** (1.69 eV), **8d** (1.07 eV) to **7d** (0.88 eV), supporting the anodic shift of the first reduction potential along this series (see Table 1). The energy of the HOMO remains mostly unaffected, justifying the almost identical oxidation potentials recorded for compounds **6**–**8**.

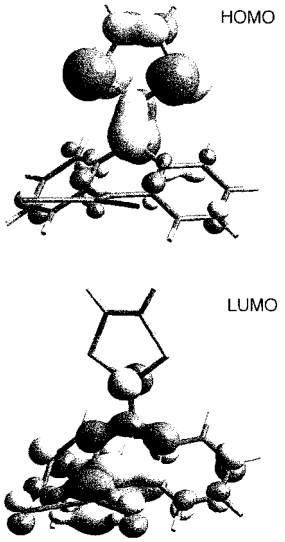

Figure 9. Electron density contours of the HOMO and LUMO of **7d**.

The AO composition of the HOMO and LUMO of the donor–acceptor compounds **6**, **7** and **8** indicates that the lowest energy HOMO→LUMO electronic transition involves an electron transfer from the dithiole group to the acceptor part of the molecule. This supports the intramolecular charge-transfer character of the longest wavelength absorption band observed in the electronic spectra. The HOMO–LUMO energy gap decreases with the acceptor ability of the electron-withdrawing group (**6** > **8** > **7**) owing to the stabilisation of the LUMO. This trend mirrors the bathochromic shift observed experimentally along that series, especially passing from **6** to **7** and **8** (see Table 1). For compound **11**, the lowest energy absorption band has no charge-transfer character, since both the HOMO and the LUMO are mostly located on the 1,3-dithiol-2-ylidene units; this supports the assignment of the observed electronic spectra. It is to be noted that no significant charge transfer is found for compounds **6**, **7** and **8** in the ground state. While each of the dithiole rings in **11d** bears a net atomic charge of −0.044 e, this ring has a charge of −0.012 e in **6d**, −0.009 e in **8d** and 0.013 e in **7d**. This means that there is a maximum charge transfer from the dithiole ring of 0.057 e for **7d** in its ground state. This charge transfer is small compared with that obtained for other 1,3-dithiole based donor–acceptor compounds, where a conjugated π spacer separates the donor and the acceptor units.[29] The absence of conjugation in compounds **6**, **7** and **8**, due to the boat conformation adopted by the anthracene spacer is likely to be the cause of this diminished charge transfer in the ground state.

Charged compounds: To get a deeper understanding of the oxidation and reduction processes, the molecular geometries of the radical cation, radical anion and dianion of **7d** were optimised at the ab initio 6–31G* level. The most relevant bond lengths calculated for these species are included in Table 4 to be compared with those obtained for neutral **7d**. The oxidation process affects the 1,3-dithiol-2-ylidene moiety, as suggested above on the basis of the AO composition of the

HOMO. The S–C bonds shorten to 1.72 Å and the exocyclic C(11)–C(9) double bond lengthens to 1.40 Å. The remaining bond lengths remain almost unaffected by the loss of an electron. In a similar way, reduction mainly affects the $C{=}C(CN)_2$ unit and leaves the dithiole group unchanged. The parameter that undergoes the largest modification in passing to the anion is the exocyclic C(10)–C(16) bond, which lengthens from 1.347 to 1.436 Å. As a whole, the anthracene backbone is slightly more affected by reduction than by oxidation. This effect can be attributed to the more significant contributions that the anthracene moiety makes to the LUMO (see Figure 9).

The lengthening of the exocyclic C(11)–C(9) bond for the cation and of the C(10)–C(16) bond for the anion lowers the steric contacts of the *peri* hydrogen atoms with the sulfur atoms and with the cyano groups, respectively. However, the relaxation of the steric hindrance reduces only slightly the distortions from planarity, because it only acts on one side of the molecule. The dihedral angle formed by the outer benzene rings changes from 41.8° for neutral **7d** to 40.5° for $\mathbf{7d}^{+\bullet}$ and to 38.6° for $\mathbf{7d}^{-\bullet}$. The folding of the central ring along the C(8a)–C(9a) vector (35.4° for **7d**) slightly diminishes for $\mathbf{7d}^{+\bullet}$ (34.1°) and increases for $\mathbf{7d}^{-\bullet}$ (36.3°), while that along the C(4a)–C(10a) vector (34.6° for **7d**) remains unchanged for the radical cation (34.5°) and reduces to 27.6° for the radical anion.

The attachment of the second electron to form the dianion of **7d** affects the whole molecule but mainly causes changes to the surroundings of the exocyclic C(10)–C(16) bond, which now has a length of 1.50 Å. The marked single-bond character of this bond causes the dicyanomethylene group to rotate to the perpendicular twisted structure displayed in Figure 10.

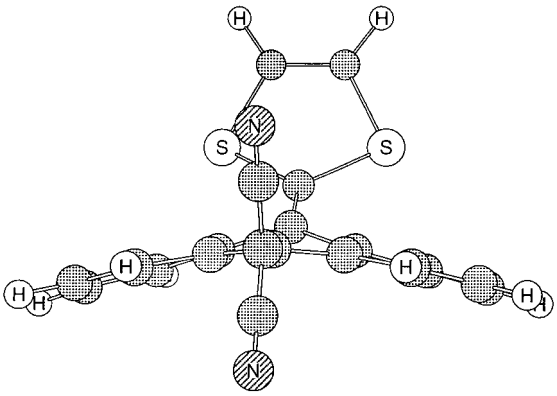

Figure 10. Molecular conformation calculated at the ab initio 6–31G* level for $\mathbf{7d}^{2-}$.

This conformation avoids the steric interactions of the cyano groups with the *peri* hydrogens and is calculated to be 14.17 kcal mol^{-1} more stable than the optimised butterfly conformation, which is analogous to that shown by neutral **7d** and the radical anion $\mathbf{7d}^{-\bullet}$. Calculations for both the radical anion and the radical cation of **7d** with either the $C(CN)_2$ group ($\mathbf{7d}^{-\bullet}$) or the dithiole ring ($\mathbf{7d}^{+\bullet}$) in a perpendicular position indicated that they are 5.39 and 10.11 kcal mol^{-1} less stable than the respective butterfly-shaped conformations.

Despite the absence of steric interactions on the acceptor side of the molecule, the anthracene moiety of $\mathbf{7d}^{2-}$ remains significantly distorted from planarity, due to the S–H_{peri} contacts present on the donor side. This asymmetry results in a small folding of 10.4° along the C(4a)–C(10a) vector, while a folding of 28.2° is still present along the C(8a)–C(9a) vector. As a consequence, the outer benzene rings are no longer planar and exhibit distortions of 9–10°. They form an average dihedral angle of approximately 24°, significantly smaller than that of neutral **7d** (41.8°) and $\mathbf{7d}^{-\bullet}$ (38.6°). For $\mathbf{7d}^{2-}$, the dithiole ring is more bent along the S–S vector (28.8°) than in **7d** (7.1°) and in $\mathbf{7d}^{-\bullet}$ (16.1°), due to the shorter S–H_{peri} contacts (2.59 Å) present in $\mathbf{7d}^{2-}$. The structural asymmetry calculated for the anthracene unit of $\mathbf{7d}^{2-}$ is also shown in Figure 11, where it is compared with that for the anthracene molecule. While the lower part connected to the $C(CN)_2$ unit has gained in aromaticity and strongly resembles that of anthracene, the upper part clearly differs. The anthracene unit of $\mathbf{7d}^{2-}$ thus shows a molecular structure intermediate between aromatic anthracene and the two independent benzene rings present in neutral **7d**.

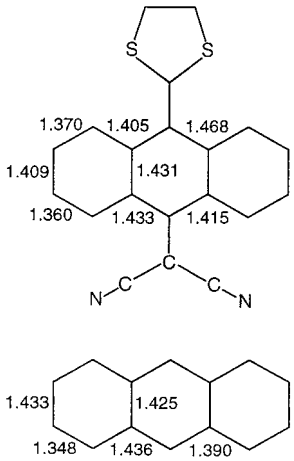

Figure 11. 6–31G* optimised bond lengths [Å] for the central anthracene unit of $\mathbf{7d}^{2-}$ (top) and for the anthracene molecule (bottom).

The Mulliken net atomic charge distributions calculated for **7d**, $\mathbf{7d}^{-\cdot}$ and $\mathbf{7d}^{2-}$ indicate that the first extra electron is mostly accommodated by the $C(CN)_2$ group (0.42 e) and by the hydrogen atoms of the anthracene unit (0.28 e). The second electron is located in the $C(CN)_2$ unit (0.31 e), the hydrogen atoms of the anthracene unit (0.31 e) and the dithiole ring (0.32 e). The population analysis thus suggests that the second reduction wave, observed in the cyclic voltammogram of compounds **7**, should not be ascribed to the reduction of the anthracene moiety, since the net charge of the anthracene carbon backbone remains almost unchanged during the charging process. The total electron density gained by the $C(CN)_2$ group in passing from **7d** to $\mathbf{7d}^{2-}$ (0.73 e) is in fact very similar to the extra charge of 0.71 e accumulated by each of the $C(CN)_2$ units in the dianion of the acceptor molecule 11,11,12,12-tetracyano-9,10-anthraquinodimethane (TCAQ).[30] For TCAQ, which also exhibits a butterfly structure in the neutral state,[30, 31] the introduction of the second electron to form the dianion completes the planarisation, that is the aromatisation, of the anthracene moiety and the reduction of this moiety takes place during the formation of the trianion and tetraanion.[30, 32] For compounds **6**, **7** and **8**, the aromatisation of the anthracene backbone is hampered by the presence of the donor unit, which hinders it from achieving planarity in the reduction process.

0947-6539/98/0412-2588 $ 17.50+.50/0 *Chem. Eur. J.* **1998**, *4*, No. 12

Conclusion

In summary, we have prepared a variety of extended donor–acceptor (**6**, **7** and **8**) and donor–donor **11** species based on an anthracenediylidene backbone. The electronic absorption spectra of the donor–acceptor compounds exhibit an intramolecular charge-transfer band, which is sensitive to the nature of both the donor and acceptor groups. The steady-state emission observed from these compounds is weak, exhibiting solvent dependence in both band position and intensity. Preliminary time-resolved spectroscopic studies indicate that at least two excited states may form on photolysis and that the lifetime of 170–400 ps is strongly dependent on solvent polarity. Cyclic voltammetric studies establish that both radical cations and radical anions can be generated in solution by one-electron oxidation and reduction, respectively. The highly distorted geometry of the neutral species has been established by X-ray crystal structure analysis and by ab initio theoretical calculations. The molecules exhibit a butterfly-shaped structure, in which the central quinone-type ring adopts a boat conformation and the outer benzene rings are tilted in the opposite direction and preserve their planarity. The degree of distortion from planarity is determined by the steric contacts of the hydrogen atoms in *peri* positions with the donor/acceptor units. The energies and topologies of the HOMO and the LUMO afford a first explanation of the redox properties and support the intramolecular charge-transfer nature of the lowest energy absorption band, observed experimentally for compound **6**, **7** and **8**. The oxidation and reduction processes have been studied in more detail by optimising the molecular structure of the radical cation, radical anion and dianion of compound **7**. While oxidation affects the 1,3-dithiole environment, reduction changes the C=C(CN)$_2$ unit. For the dianion, the C=C(CN)$_2$ group is twisted around the exocyclic C=C bond and the central anthracene backbone becomes less distorted from planarity. The presence of the donor 1,3-dithiole unit hampers the achievement of a fully planar aromatic anthracene structure.

Experimental Section

General details: ^{1}H NMR spectra were obtained using Varian instruments VXR 200 operating at 199.98, 299.907, or 399.958 MHz. Variable temperature ^{1}H NMR spectra and ^{13}C NMR spectra (100.581 MHz) were obtained using a Varian 400 spectrometer. Mass spectra were recorded using a VG7070E spectrometer operating at 70 eV. IR spectra were recorded using a Perkin-Elmer 1615 FTIR spectrometer operating from a Grams analyst 1600. Melting points were obtained by using a Kofler hot stage microscope apparatus and are uncorrected. Cyclic voltammetry measurements were performed on a EG&G PAR Versastat potentiostat using 250 Electrochemical Analysis software. A Metrohm 6.0804.C10 glassy carbon electrode was used as indicator electrode in voltammetric studies (1×10^{-5} M solutions of the compound in dichloromethane, 0.1 M Bu_4NClO_4 as the supporting electrode, platinum working and counter electrode, SCE as reference electrode at 20 °C). All chromatography was performed using Merck silica gel (70–230 mesh). All reagents were used as purchased unless otherwise stated. All solvents were dried according to standard procedures. All reactions were carried out under an atmosphere of dry argon.

A Hitachi U-3000 spectrophotometer and a Shimadzu RF-150X spectrofluorimeter were used for UV/visible absorption and emission studies, respectively. Samples were contained in 10 mm pathlength cells and all studies were carried out at room temperature (approximately 18 °C). The ultrafast apparatus has been described in detail elsewhere.[33, 34] Briefly, the output of an amplified dye laser system (606 nm, 50 μJ, 200 fs, 1050 Hz) provided photolysis pulses in the visible or in the UV by frequency doubling (303 nm, 1.4–1.8 μJ), and probe pulses (400–800 nm) by white light continuum generation. The continuum probe was focused to a diameter of approximately 200 μm in the sample cell, coincident with the photolysis beam, which was focused to a diameter of approximately 250 μm using near collinear geometry. The pump beam was synchronously chopped at 525 Hz. The emerging beam was analysed using 10 nm bandpass interference filters and a photodiode coupled to lock-in amplifiers. In all cases, the relative polarisation of the pump and probe beams was set at the 'magic angle' of 54.7°. A stoppered 1 mm pathlength quartz cell containing the sample solution was translated rapidly in two directions perpendicular to the laser beams at a rate sufficient to ensure that each pulse pair encountered fresh sample.[35] UV/visible absorption spectra measured before and after the laser experiments confirmed the integrity of the samples.

Computational procedure: All the calculations were performed at the ab initio Hartree–Fock (HF) level using the 6–31G* basis set,[36] which includes polarisation *d* functions on heavy atoms, and the GAUSSIAN 94 program.[37] Neutral molecules and dianions were computed within the restricted HF (RHF) formalism. The geometries of the singly charged cations and anions were calculated using both the restricted open-shell HF (ROHF) formalism and the spin-unrestricted HF (UHF) approximation.[38] In the latter, electrons with different spins occupy different sets of orbitals. Only the results obtained using the ROHF procedure are given, because both approaches led to similar geometries, but the latter presents a high-spin contamination, $S^2=2.328$ instead of the value of 0.75 typical of a doublet. Geometry optimisations were carried out using the Berny analytical gradients method.[39] The requested convergence on the density matrix was 10^{-8} and the threshold values for the maximum force and the maximum displacement in the optimisation process were 0.00045 and 0.0018 atomic units, respectively. The calculations were performed on IBM RS/6000 workstations and on a SGI Power Challenge L R8000 computer at the Department of Química Física of the University of València.

X-ray crystallography: Single-crystal X-ray diffraction experiments for **6a** and **11a** were carried out on a Rigaku AFC6S four-circle diffractometer, for **7b** on a Siemens SMART 3-circle diffractometer with a CCD area detector (with a Cryostream open-flow N_2 gas cryostat[40]), using graphite-monochromated $Mo_{K\alpha}$ radiation ($\lambda=0.71073$ Å). For **6a** and **11a**, empirical (ψ scans) absorption corrections[41] were applied, using TEXSAN software.[42] All three structures were solved by direct methods, using SHELXS-86 programs.[43] Structures **6a** and **11a** were refined by full-matrix least squares against F of observed data with $w^{-1}=\sigma^2(F)+0.0002F^2$ weights (SHELXTL PLUS software[44]), and **7b** against F^2 of all data with two term weighting scheme (SHELXL-93 software[45]). Non-hydrogen atoms were refined anisotropically; in **6a** all H atoms were refined isotropically, in **7b** and **11a** methyl groups were refined as rigid bodies, other H atoms were treated as 'riding'. In **11a**, one methyl group is disordered; the C(15) atom occupies two positions, A and B (both refined in isotropic approximation with 50% occupancies), but two of the H atoms occupy essentially the same positions for both orientations of C(15). Crystal data and experimental details are listed in Table 3. Crystallographic data (excluding structure factors) for the structures reported in this paper have been deposited with the Cambridge Crystallographic Data Centre as supplementary publication nos. CCDC-101940 (**6a**), CCDC-101941 (**7b**), CCDC-101942 (**11a**). Copies of the data can be obtained free of charge on application to CCDC, 12 Union Road, Cambridge CB2 1EZ, UK (fax: (+44) 1223-336-033; e-mail: deposit@ccdc.cam.ac.uk).

10-(4,5-Dimethylthio-1,3-dithiol-2-ylidene)anthracene-9(10H)one (**6a**): To a solution of sodium ethoxide [prepared from finely grated sodium (0.21 g, 8.9 mmol) in dry ethanol (50 mL)] was added anthrone **5** (1.71 g, 8.8 mmol) and the resulting yellow solution was stirred for 15 mins. After this time, 2,4,5-tri(methylthio)-1,3-dithiolium tetrafluoroborate **4a**[12] (3.0 g, 8.8 mmol) was added and the solution was warmed to 60 °C for 16 h. The solution was then allowed to cool and the precipitated solid was filtered and purified by column chromatography, eluent dichloromethane/cyclohexane

1:1 (v/v) to afford compound **6a** as an orange solid (1.71 g, 50%; m.p. 185 °C (from cyclohexane/dichloromethane)). Elemental analysis calcd. for $C_{19}H_{14}OS_4$: C 59.04, H 3.65; found C 58.85, H 3.96. *m/z* (DCI): 386 [M^+]; ^{1}H NMR ($CDCl_3$, 200 MHz): $\delta = 8.27$ (d, 2H, $J = 7.5$ Hz), 7.79 (d, 2H, $J =$ 7.5 Hz), 7.65 (t, 2H, $J = 7.5$ Hz), 7.44 (t, 2H, $J = 7.5$ Hz), 2.42 (s, 6H,); ^{13}C NMR ($CDCl_3$): $\delta = 184.0$, 140.6, 139.1, 132.3, 131.2, 127.8, 127.4, 127.3, 126.7, 119.9, 19.8; IR (KBr) (cm^{-1}): 1650 (CO), 1600, 1495, 1470, 1445, 1300, 1170, 940, 780, 700; UV/vis (CH_2Cl_2): λ_{max} (ε) (nm): 468 (1.3×10^4), 360 (6.2×10^3), 250 (3.4×10^4).

10-(4,5-dimethyl-1,3-dithiol-2-ylidene)anthracene-9-(10H)one (**6b**): This compound was prepared according to a modified literature procedure,[9] in which anthrone **5** (3.83 g, 19.7 mmol) was added to a stirred solution of pyridine/acetic acid (100 mL, 3:1 v/v), 4,5-dimethyl-2-methylthio-1,3-dithiolium iodide **4b** (6.0 g, 19.7 mmol) was added and the solution warmed to 50–60 °C for 16 h. The volume of solvent was reduced in vacuo to approximately 50 mL, when a red solid precipitated. This solid was filtered, washed with hexane, taken up in dichloromethane and the resulting white precipitate removed by filtration. The filtrate was concentrated in vacuo to yield compound **6b** as a red crystalline solid (3.7 g, 60%; m.p. 222–224 °C (ref. [9] 217–218 °C)). Spectroscopic and analytical measurements were entirely consistent with those reported previously for compound **6b**.[9]

10-[4,5-(Ethylenedithio)-1,3-dithiol-2-ylidene]anthracene-9-(10H)one (**6c**): This compound was prepared in a similar way to **6b** using 4,5-ethylenedithio-2-methylthio-1,3-dithiolium tetrafluoroborate **4d** and isolated as a red solid in 69% yield (m.p. 201–203 °C). Elemental analysis calcd. for $C_{19}H_{12}OS_4$: C 59.35, H 3.15; found C 59.49, H 3.02. *m/z* (EI): 384 ([M^+], 100). ^{1}H NMR ($CDCl_3$, 300 MHz): $\delta = 8.27$ (d, 2H, $J = 8$ Hz), 7.74, (d, 2H, $J = 8$) 7.66 (t, 2H, $J = 8$ Hz), 7.45 (t, 2H, $J = 8$ Hz), 3.33 (s, 4H); ^{13}C NMR ($CDCl_3$): $\delta = 153.7$, 138.7, 138.1, 136.4, 135.4, 131.7, 130.5, 127.1, 126.8, 126.2; IR (KBr) (cm^{-1}): 1640 (CO), 1595, 1490, 1470, 1440, 1290, 1200, 1160, 930, 770, 690; UV/vis (CH_2Cl_2): λ_{max} (ε) (nm): 482 (1.0×10^4), 378 (5.2×10^3), 252 (3.9×10^4).

10-(4,5-Dihydro-1,3-dithiol-2-ylidene)anthracene-9-(10H)-one (**6d**). This compound was prepared by a literature procedure[13b] in 86% yield.

Synthesis of the dicyanovinyl derivatives 7a–d. General procedure: To a stirred solution of the corresponding ketone **6a–d** (1 equiv) in dry chloroform was added sequentially malononitrile (10 equiv), titanium tetrachloride (1M in CH_2Cl_2, 2.5 equiv) and finally, dry pyridine (10 equiv). The resulting blue/black solution was refluxed for 20 h. The solution was then allowed to cool and the solvent removed in vacuo to leave a residue, which was purified by column chromatography using dichloromethane as eluent.

10-(4,5-Dimethylthio-1,3-dithiol-2-ylidene)-9-(2,2-dicyanomethylene)anthracene (**7a**): From ketone **6a** (0.104 g, 0.27 mmol), dry chloroform (50 mL), malononitrile (0.178 g, 2.7 mmol), $TiCl_4$ (0.68 mL, 0.68 mmol) and dry pyridine (0.23 mL, 2.8 mmol), **7a** was obtained as a purple solid (0.08 g, 65%); m.p. 250 °C (decomp). Elemental analysis calcd. for $C_{22}H_{14}N_2S_4$: C 60.80, H 3.25, N 6.45; found C 61.02, H 3.56, N 6.54. *m/z* (EI): 434 ([MH^+], 100). ^{1}H NMR ($CDCl_3$, 200 MHz): $\delta = 8.14$ (dd, 2H, $J_1 = 7.9$, $J_2 = 1.1$ Hz), 7.80 (dd, 2H, $J_1 = 7.9$, $J_2 = 1.1$ Hz), 7.59 (td, 2H, $J_1 = 7.9$, $J_2 = 1.1$ Hz), 7.44 (td, 2H, $J_1 = 7.9$, $J_2 = 1.1$ Hz), 2.42 (s, 6H); ^{13}C NMR ($CDCl_3$): $\delta = 162.4$, 140.1, 135.0, 131.4, 128.6, 127.0, 126.8, 126.5, 125.7, 119.8, 114.8, 19.8; IR (KBr) (cm^{-1}): 2240, 1600, 1570, 1530, 1500, 1350, 1300, 1200, 1120, 720, 700, 680; UV/vis (CH_2Cl_2): λ_{max} (ε) (nm): 545 (3.5×10^3), 243 (5.6×10^4).

10-(4,5-Dimethyl-1,3-dithiol-2-ylidene)-9-(2,2-dicyanomethylene)anthracene (**7b**): From ketone **6b** (0.16 g, 0.5 mmol), dry chloroform (20 mL), malononitrile (0.33 g, 5.0 mmol), $TiCl_4$ (0.42 mL, 0.42 mmol), dry pyridine (0.40 mL, 5.0 mmol). **7b** was obtained as a purple solid (0.122 g, 66%; m.p. 250 °C (decomp)). Slow evaporation of a dichloromethane/hexane solution (1:1 v/v) of compound **7b** yielded X-ray quality crystals. Elemental analysis calcd. for $C_{22}H_{14}N_2S_2$: C 71.32, H 3.81, N 7.56; found C 71.54, H 3.66, N 7.85. *m/z* (EI): 370 ([M^+], 100). ^{1}H NMR ($CDCl_3$, 200 MHz): $\delta = 8.14$ (dd, 2H, $J_1 = 7.9$, $J_2 = 1.1$ Hz), 7.94 (dd, 2H, $J_1 = 7.9$, $J_2 = 1.1$), 7.80 (td, 2H, $J_1 = 7.9$, $J_2 = 1.1$ Hz), 7.39 (td, 2H, $J_1 = 7.9$, $J_2 = 1.1$ Hz), 2.04 (s, 6H,); ^{13}C NMR ($CDCl_3$): $\delta = 162.2$, 143.6, 135.5, 131.2, 128.4, 126.3, 126.2, 125.6, 122.5, 116.8, 115.1, 13.1; IR (KBr) (cm^{-1}): 2240, 1600, 1565, 1530, 1500, 1450, 1295, 1210, 1175, 820, 780, 700, 685. UV/vis (CH_2Cl_2): λ_{max} (ε) (nm): 572 (1.1×10^4), 231 (3.2×10^3).

10-[4,5-(Ethylenedithio)-1,3-dithiol-2-ylidene]-9-(2,2-dicyanomethylene) anthracene (**7c**): From ketone **6c** (0.17 g, 2.6 mmol), dry chloroform (30 mL), malononitrile (0.17 g, 2.6 mmol), $TiCl_4$ (0.65 mL, 0.65 mmol) and dry pyridine (0.15 mL, 1.8 mmol), **7c** was obtained as a purple solid (0.06 g, 54%); m.p. > 250 °C (decomp). Elemental analysis calcd. for $C_{22}H_{12}N_2S_4$: C 61.11, H 2.77, N 6.45; found C 61.24, H 3.01, N 6.50; *m/z* (EI): 432 ([M^+], 100). ^{1}H NMR ($CDCl_3$, 300 MHz): $\delta = 8.13$ (dd, 2H, $J_1 =$ 7.8, $J_2 = 1.2$ Hz), 7.78 (dd, 2H, $J_1 = 7.8$, $J_2 = 1.2$ Hz), 7.59 (td, 2H, $J_1 = 7.8$, $J_2 = 1.2$ Hz), 7.43 (td, 2H, $J_1 = 7.8$, $J_2 = 1.2$ Hz), 3.35 (s, 4H). ^{13}C NMR ($CDCl_3$): $\delta = 162.2$, 143.6, 135.0, 131.2, 128.5, 126.8, 126.4, 125.7, 122.5, 114.7, 111.8, 29.34; IR (KBr) (cm^{-1}): 2220, 1600, 1570, 1540, 1500, 1450, 1295, 1205, 810, 780, 700; UV/vis (CH_2Cl_2): λ_{max} (ε) (nm): 560 (7.6×10^3), 332 (1.2×10^4), 258 (1.5×10^4), 232 (1.8×10^4).

10-(4,5-dihydro-1,3-dithiol-2-ylidine)-9-(2,2-dicyanomethylene)anthracene (**7d**): From ketone **6d** (0.17 g, 0.35 mmol), dry chloroform (50 mL), malononitrile (0.17 g, 2.6 mmol), $TiCl_4$ (0.85 mL, 0.85 mmol) and dry pyridine (0.23 mL, 2.8 mmol), **7c** was obtained as a black solid (0.09 g, 84%); m.p. 199–201 °C; elemental analysis calcd. for $C_{20}H_{10}N_2S_2$: C 70.15, H 2.94, N 8.18; found C 69.88, H 3.21, N 7.98. *m/z* (EI): 342 ([M^+], 100). ^{1}H NMR ($CDCl_3$, 300 MHz): $\delta = 8.13$ (dd, 2H, $J_1 = 7.8$, $J_2 = 1.2$ Hz) 7.98, (dd, 2H, $J_1 = 7.8$, $J_2 = 1.2$ Hz), 7.60 (td, 2H, $J_1 = 7.8$, $J_2 = 1.2$ Hz), 7.41 (td, 2H, $J_1 = 7.8$, $J_2 = 1.2$ Hz), 6.52 (s, 2H). ^{13}C NMR ($CDCl_3$): $\delta = 162.2$, 143.6, 139.2, 131.7, 130.4, 127.0, 126.4, 125.9, 117.9, 117.5; IR (KBr) 2240, 1600, 1570, 1535, 1490, 1445, 1290, 1265, 1200, 1170, 810, 770, 700, 685 cm^{-1}; UV/vis (CH_2Cl_2) λ_{max} (CH_2Cl_2) (ε) (nm): 542 (1.0×10^4), 245 (2.9×10^3).

Synthesis of cyanoimine derivatives 8a–d. General procedure: To a stirred solution of the corresponding ketone (**6a–d**) (1 equiv) in dry chloroform was added titanium tetrachloride (1M in CH_2Cl_2, 3.5 equiv) followed by *N*,*N*-bis(trimethylsilyl)carbodiimide (BTC) (3 equiv). The resulting dark solutions were heated under reflux for 48–72 h with periodic addition of more BTC until no starting material was observable (TLC analysis). The solution was allowed to cool, the solvent removed in vacuo and the residue purified by silica gel chromatography, to afford compounds **8a–d**.

9-(4,5-Dimethylthio-1,3-dithiol-2-ylidene)-10-*N*-cyanoimine anthracene (**8a**): From ketone **6a** (0.14 g, 0.36 mmol), dry chloroform (20 mL), $TiCl_4$ (1.27 mL, 1.27 mmol) and BTC (0.24 mL, 1.06 mmol), with eluent CH_2Cl_2, **8a** was obtained as a blue/black solid (0.05 g, 47%; m.p. 175–178 °C). Elemental analysis calcd. for $C_{20}H_{14}N_2S_4$: C 58.51, H 3.44, N 6.82; found C 58.63, H 3.22, N 6.91. *m/z* (DCI): 411 ([MH^+], 100). ^{1}H NMR ($CDCl_3$, 400 MHz, −30 °C): $\delta = 8.83$ (d, 1H, $J = 7.6$ Hz), 8.21 (d, 1H, $J = 7.6$ Hz), 7.85 (d, 1H, $J = 7.6$ Hz), 7.74–7.67 (m, 3H), 7.52 (t, 1H, $J = 7.6$ Hz), 7.45 (t, 1H, $J = 7.6$ Hz), 2.42 (s, 6H); ^{13}C NMR ($CDCl_3$): $\delta = 173.3$, 142.4, 136.9, 132.4, 127.4, 127.0, 126.8, 126.0 (2C, broad), 119.2, 115.6, 19.3; IR (KBr) (cm^{-1}): 2150, 1600, 1570, 1530, 1485, 1430; UV/vis (CH_2Cl_2): λ_{max} (ε) (nm): 542 (8.5×10^3), 232 (2.6×10^3).

9-(4,5-Dimethyl-1,3-dithiol-2-ylidine)-10-*N*-cyanoimine anthracene (**8b**): From ketone **6b** (0.1 g, 0.31 mmol), dry chloroform (30 mL), $TiCl_4$ (1.1 mL, 1.1 mmol) and BTC (0.20 mL, 0.89 mmol), with eluent CH_2Cl_2, **8b** was obtained as a blue–black solid (0.09 g, 85%; m.p. 234–236 °C). Elemental analysis calcd. for $C_{20}H_{14}N_2S_2$: C 69.36, H 4.04, N 8.09; found C 69.44, H 4.20, N 7.82; *m/z* (EI): 346 ([M^+], 100). ^{1}H NMR ($CDCl_3$, 300 MHz): $\delta = 8.00–7.88$ (m, 2H), 7.91–7.85 (m, 2H), 7.66 (td, 2H, $J_1 = 7.8$, $J_2 = 1.2$ Hz), 7.43 (t, 2H, $J = 7.8$ Hz), 2.04 (s, 6H); ^{13}C NMR ($CDCl_3$): $\delta =$ 162.2, 143.6, 137.2, 132.0, 128.8, 126.5, 126.0, 125.8, 122.8, 116.0, 115.9, 108.0, 12.9; IR (KBr) (cm^{-1}): 2150, 1600, 1570, 1530, 1485, 1420, 1300, 1180, 770, 685; UV/vis (CH_2Cl_2): λ_{max} (ε) (nm): 566 (2.0×10^4), 378 (1.1×10^4), 316 (1.9×10^4), 256 (2.5×10^4).

9-[4,5-(Ethylenedithio)-1,3-dithiol-2-ylidene]-10-*N*-cyanoimine anthracene (**8c**): From ketone **6c** (0.1 g, 0.26 mmol), dry chloroform (20 mL), $TiCl_4$ (0.86 mL, 0.86 mmol) and BTC (0.12 mL, 0.53 mmol), with eluent CH_2Cl_2, **8c** was obtained as a blue–black solid (0.08 g, 77%; m.p. 178–179 °C). Elemental analysis calcd. for $C_{20}H_{12}N_2S_4$: C 58.80, H 2.96, N 6.86; found C 59.01, H 2.79, N 6.91; *m/z* (EI): 408 ([M^+], 100). ^{1}H NMR ($CDCl_3$, 300 MHz): $\delta = 8.00–7.81$ (m, 4H), 7.68 (t, 2H, $J = 7.8$ Hz), 7.47 (t, 2H, $J =$ 7.8 Hz), 3.35 (s, 4H); ^{13}C NMR ($CDCl_3$): $\delta = 161.4$, 144.6, 136.1, 131.9, 128.0, 126.2, 125.6, 123.0, 115.8, 108.0, 30.0; IR (KBr): 2150, 1600, 1570, 1545, 1485, 1420, 1300, 1200, 1170, 800, 770, 680 cm^{-1}; UV/vis (CH_2Cl_2): λ_{max} (ε) (nm): 558 (8.7×10^4), 320 (1.1×10^4), 260 (2.5×10^4).

9-(4,5-Dihydro-1,3-dithiol-2-ylidine)-10-*N*-cyanoimine anthracene (**8d**): From ketone **6d** (0.1 g, 0.34 mmol), dry chloroform (50 mL), $TiCl_4$ (1.19 mL, 1.19 mmol) and BTC (0.23 mL, 1.02 mmol), with the eluent hexane:CH_2Cl_2 (5:3), **8a** was obtained as a blue–black solid (0.025 g, 23%)

0947-6539/98/0412-2590 $ 17.50+.50/0 *Chem. Eur. J.* **1998**, *4*, No. 12

m.p. 185–186 °C. Elemental analysis calcd. for $C_{18}H_{10}N_2S_2$: C 67.92, H 3.14, N 8.80; found C 68.01, H 3.00, N 8.95. *m/z* (DCI): 319 ([MH^+], 100). ^{1}H NMR ($CDCl_3$, 400 MHz, −30 °C): $\delta = 8.85$ (d, 1H, $J = 8.0$ Hz), 8.23 (d, 1H, $J = 8.0$ Hz), 8.01 (d, 1H, $J = 8.0$ Hz), 7.93 (d, 1H, $J = 8.0$ Hz), 7.71 (t, 1H, $J = 8.0$ Hz), 7.70 (t, 1H, $J = 8.0$ Hz), 7.48 (t, 1H, $J = 8.0$ Hz), 7.43 (t, 1H, $J = 8.0$ Hz), 6.59 (s, 2H); ^{13}C NMR ($CDCl_3$): $\delta = 173.3$, 147.7, 137.6, 134.3, 132.4, 127.3, 126.7, 125.8 (broad), 118.5, 117.5, 115.8; IR (KBr): 2155 cm^{-1}; UV/vis (CH_2Cl_2): λ_{max} (ε) (nm): 543 (1.5×10^4), 229 (1.7×10^3).

9,10-Bis(4,5-dimethylthio-1,3-dithiol-2-ylidene)-9,10-dihydroanthracene (11a): To a solution of phosphonate ester **7**[13] (0.9 g, 3 mmol) in anhydrous tetrahydrofuran (20 mL) at −78 °C was added *n*BuLi (1.6 M in hexane, 2 mL, 3.2 mmol). After 0.5 h at this temperature, a solution of anthraquinone (0.3 g, 1.4 mmol) in tetrahydrofuran (10 mL) was added and the solution was stirred for 1 h at −78 °C before warming to room temperature overnight. The solvent was then removed in vacuo, dichloromethane (100 mL) was added and the organic phase was washed with water (2 × 100 mL), dried ($MgSO_4$) and evaporated to yield a yellow solid, which was purified by column chromatography, with the eluent hexane/dichloromethane (2:1 v/v) to yield compound **11a** as a yellow solid (0.31 g, 38 %; m.p. > 230 °C.) Recrystallisation from acetonitrile/dichloromethane afforded crystals for X-ray analysis. Elemental analysis calcd. for $C_{24}H_{20}S_8$: C 51.0, H 3.57; found C 50.9, H 3.54; *m/z* (EI): 564 ([M^+], 100). ^{1}H NMR ($CDCl_3$, 200 MHz): $\delta = 7.54$ and 7.32 (each 4H, first order AA′XX′, all *ortho* $J_{H,H}$ 8.0), 2.40 (12H, s).

9,10-Bis(4,5-dimethyl-1,3-dithiol-2-ylidene)-9,10-dihydroanthracene (11b): This compound was prepared according to the published procedure.[13b]

Acknowledgments: The groups from Madrid and Valencia jointly acknowledge financial support by the CICYT Grant PB95-0428-C02. The work in York was funded by EPSRC, through research grant and Advanced Fellowship (J. N. M.) awards. The work in Durham was funded by EPSRC (A. S. B., M. C., A. J. M. and A. G.), Zeneca Specialties (A. G.), Leverhulme scholarship (A. S. B.), Royal Society visiting fellowship (A. S. B.) and EC HCM Program CHRX-CT93-0271 (M. S.). M. R. B. thanks the University of Durham for a Sir Derman Christopherson Research Fellowship.

Received: May 13, 1998 [F1155]

[1] a) R. W. Boyd, *Nonlinear Optics*, Academic Press, New York, **1992**; b) P. N. Prasad, D. J. Williams, *Introduction to Nonlinear Optical Effects in Molecules and Polymers*, Wiley, New York, **1991**; c) H. S. Nalwa, *Adv. Mater.* **1993**, *5*, 341–358; d) N. J. Long, *Angew. Chem.* **1995**, *Angew. Chem. Int. Ed. Engl.* **1995**, *34*, 21–38; e) R. G. Denning, *J. Mater. Chem.* **1995**, *5*, 365–378; f) M. S. Wong, C. Bossard, P. Günter, *Adv. Mater.* **1997**, *9*, 837–842; g) T. Verbiest, S. Houbrechts, M. Kauranen, K. Clays, A. Persoons, *J. Mater. Chem.* **1997**, *7*, 2175–2189.

[2] a) R. M. Metzger, C. Panetta, *New J. Chem.* **1991**, *15*, 209–221; b) *An Introduction to Molecular Electronics*, (Eds.: M. C. Petty, M. R. Bryce, D. Bloor), Oxford University, New York, **1995**.

[3] H. Kurreck, M. Huber, *Angew. Chem.* **1995**, *Angew. Chem. Int. Ed. Engl.* **1995**, *34*, 849–866.

[4] F. Effenberger, F. Würthner, F. Steybe, *J. Org. Chem.* **1995**, *60*, 2082–2091.

[5] a) R. A. Marcus, *Rev. Mod. Phys.* **1993**, *65*, 599–610; b) M. N. Paddon-Row, *Acc. Chem. Res.* **1994**, *27*, 18–25; c) A. F. Perepichka, A. F. Popov, T. V. Orekova, M. R. Bryce, A. N. Vdovichenko, A. S. Batsanov, L. M. Goldenberg, J. A. K. Howard, N. I. Sokolov, J. L. Megson, *J. Chem. Soc. Perkin Trans. 2* **1996**, 2453–2469.

[6] a) P. Bando, N. Martín, J. L. Segura, C. Seoane, E. Ortí, P. M. Viruela, R. Viruela, A. Albert, F. H. Cano, *J. Org. Chem.* **1994**, *59*, 4618–4629; b) B. Illescas, N. Martín, J. L. Segura, C. Seoane, E. Ortí, P. M. Viruela, R. Viruela, *J. Org. Chem.* **1995**, *60*, 5643–5650; c) B. Illescas, N. Martín, J. L. Segura, C. Seoane, E. Ortí, P. M. Viruela, R. Viruela, *J. Mater. Chem.* **1995**, *5*, 1563–1570. For a recent review on molecules exhibiting photoinduced charge-transfer properties, see: N. Martín, C. Seoane in *Handbook of Organic Conductive Molecules and Polymers*, *Vol. 1* (Ed.: H. S. Nalwa), Wiley, **1997**, p. 2–82.

[7] a) N. Martín, M. Hanack, *J. Chem. Soc. Chem. Commun.* **1988**, 1522–1524; b) N. Martín, R. Benish, M. Hanack, *J. Org. Chem.* **1989**, *54*, 2563–2568; c) P. de la Cruz, N. Martín, F. Miguel, C. Seoane, A. Albert, F. H. Cano, A. González, J. M. Pingarrón, *J. Org. Chem.* **1992**, *57*, 6192–6198; d) E. Ortí, R. Viruela, P. M. Viruela, *J. Mater. Chem.* **1995**, *5*, 1697–1705. For a recent review on electron acceptor molecules, see: N. Martín, J. L. Segura, C. Seoane, *J. Mater. Chem.* **1997**, *7*, 1661–1676.

[8] a) M. R. Bryce, A. J. Moore, *Synth. Met.* **1988**, *27*, 557–561; b) M. R. Bryce, A. J. Moore, M. Hasan, G. J. Ashwell, A. T. Fraser, W. Clegg, M. B. Hursthouse, A. I. Karaulov, *Angew. Chem.* **1990**, *Angew. Chem. Int. Ed. Engl.* **1990**, *29*, 1450–1452; c) M. R. Bryce, *J. Mater. Chem.* **1995**, *5*, 1481–1496.

[9] R. Gompper, H.-U. Wagner, E. Kutter, *Chem. Ber.* **1968**, *101*, 4123–4143.

[10] S. Inoue, Y. Aso, T. Otsubo, *J. Chem. Soc. Chem. Commun.* **1997**, 1105–1106.

[11] T. Kawase, M. Wakabayashi, M. Oda, *Chem. Lett.* **1997**, 1057–1058.

[12] The synthesis of compounds **7a**, **7b** and **7d** was presented at the International Conference on the Science and Technology of Synthetic Metals, Snowbird, July 1996, *Synth. Met.* **1997**, *86*, 1857–1858. For an example of another anthracene derivative bearing redox groups at the 9 and 10 positions see: A. Knorr, J. Daub, *Angew. Chem.* **1997**, *Angew. Chem. Int. Ed. Engl.* **1997**, *36*, 2817–2819.

[13] a) M. R. Bryce, A. J. Moore, D. Lorcy, A. S. Dhindsa, A. Robert, *J. Chem. Soc. Chem. Commun.* **1990**, 470–472; b) A. J. Moore, M. R. Bryce, *J. Chem. Soc. Perkin Trans. 1* **1991**, 157–168.

[14] W. Lehnert, *Tetrahedron Lett.* **1970**, 4723–4724; W. Lehnert, *Synthesis* **1974**, 667–669.

[15] a) A. Aumüller, S. Hünig, *Angew. Chem.* **1984**, *Angew. Chem. Int. Ed. Engl.* **1984**, *23*, 447–448; b) For a recent review see: S. Hünig, *J. Mater. Chem.* **1995**, *5*, 1469–1479.

[16] A. J. Moore, M. R. Bryce, *Tetrahedron Lett.* **1992**, *33*, 1373–1376.

[17] W. Rettig, W. Baumann in *Photochemistry and Photophysics*, *Vol. 6* (Ed.: J. F. Rabek), CRC, Boca Raton, **1992**, p. 79.

[18] W. Rettig, *Angew. Chem.* **1986**, *Angew. Chem. Int. Ed. Engl.* **1986**, *25*, 971–988.

[19] B. Strehmel, W. Rettig, *J. Biomed. Opt.* **1996**, *1*, 98–189.

[20] U. Leinhos, W. Kuhnle, K. A. Zachariasse, *J. Phys. Chem.* **1991**, *95*, 2013–2021.

[21] P. Michel, A. Moradpour, P. Penven, L. Firlej, P. Bernire, B. Levy, S. Ravy, A. Zahab, *J. Am. Chem. Soc.* **1990**, *112*, 8285–8292.

[22] J. Hellberg, E. M. Pelchman, *Tetrahedron Lett.* **1994**, *35*, 1769–1772.

[23] F. Gerson, R. Heckendorn, D. O. Cowan, A. M. Kini, M. Maxfield, *J. Am. Chem. Soc.* **1983**, *105*, 7017–7023.

[24] J. Dong, K. Yakushi, Y. Yamashita, *J. Mater. Chem.* **1995**, *5*, 1735–1740.

[25] G. Filippini, A. Gavezotti, *Acta Crystallogr. Sect. B* **1993**, *49*, 868–880.

[26] J. L. Galigne, B. Liautard, S. Peytavin, G. Brun, M. Maurin, J. M. Fabre, E. Torreilles, L. Giral, *Acta Crystallogr. Sect. B* **1980**, *36*, 1109–1113.

[27] a) Y. Yamashita, S. Tanaka, K. Imaeda, H. Inokuchi, M. Sano, *Chem. Lett.* **1992**, 419–422; b) Y. Yamashita, S. Tanaka, K. Imaeda, H. Inokuchi, M. Sano, *J. Org. Chem.* **1992**, *57*, 5517–5522; c) Y. Yamashita, S. Tanaka, *Chem. Lett.* **1993**, 73–76; d) Y. Yamashita, K. Ono, S. Tanaka, K. Imaeda, H. Inokuchi, M. Sano, *J. Chem. Soc. Chem. Commun.* **1993**, 1803–1805.

[28] Y. Yamashita, S. Tanaka, K. Imaeda, H. Inokuchi, M. Sano, *J. Chem. Soc. Chem. Commun.* **1991**, 1132–1133.

[29] A. J. Moore, M. R. Bryce, A. S. Batsanov, A. Green, J. A. K. Howard, M. A. McKervey, P. McGuigan, I. Ledoux, E. Ortí, P. M. Viruela, R. Viruela, B. Tarbit, *J. Mater. Chem.* **1998**, *8*, 1173–1184.

[30] E. Ortí, P. M. Viruela, R. Viruela, *J. Phys. Chem.* **1996**, *100*, 6138–6146.

[31] U. Schubert, S. Hünig, A. Aumüller, *Liebigs Ann. Chem.* **1985**, 1216–1222.

[32] A. M. Kini, D. O. Cowan, F. Gerson, R. Möckel, *J. Am. Chem. Soc.* **1985**, *107*, 556–562.

[33] T.-Q. Ye, C. J. Arnold, D. I. Pattison, C. L. Anderton, D. Dukic, R. N. Perutz, R. E. Hester, J. N. Moore, *Appl. Spectrosc.* **1996**, *50*, 597–607.

[34] I. K. Lednev, T.-Q. Ye, R. E. Hester, J. N. Moore, *J. Phys. Chem.* **1996**, *100*, 13338–13341.

[35] *Handbook of Chemistry and Physics*, 49th ed., (Ed.: R. C. Weast), CRC, Cleveland, **1968**.
[36] P. C. Hariharan, J. A. Pople, *Chem. Phys. Lett.* **1972**, *16*, 217 – 219.
[37] M. J. Frisch, G. W. Trucks, H. B. Schlegel, P. M. W. Gil, B. G. Johnson, M. A. Robb, J. R. Cheeseman, T. Keith, G. A. Petersson, J. A. Montgomery, K. Raghavachari, M. A. Al-Laham, V. G. Zakrzewski, J. V. Ortiz, J. B. Foresman, J. Cioslowski, B. B. Stefanov, A. Nanayakkara, M. Challacombe, C. Y. Peng, P. Y. Ayala, W. Chen, M. W. Wong, J. L. Andres, E. S. Replogle, R. Gomperts, R. L. Martin, D. J. Fox, J. S. Binkley, D. J. Defrees, J. Baker, J. P. Stewart, M. Head-Gordon, C. González, J. A. Pople, Gaussian 94, Revision B.1, Gaussian Inc. Pittsburgh PA, **1995**.
[38] J. A. Pople, R. K. Nesbet, *J. Chem. Phys.* **1954**, *22*, 571 – 572.
[39] H. B. Schlegel, *J. Comput. Chem.* **1982**, *3*, 214 – 218.
[40] J. Cosier, A. M. Glazer, *J. Appl. Crystallogr.* **1986**, *19*, 105 – 107.
[41] A. C. T. North, D. C. Phillips, F. S. Mathews, *Acta Crystallogr. Sect. A* **1968**, *24*, 351 – 359.
[42] TEXSAN: Single Crystal Structure Analysis Software, Version 5.0, Molecular Structure Corporation, TX, USA, **1989**.
[43] G. M. Sheldrick, *Acta Crystallogr. Sect. A* **1990**, *46*, 467 – 473.
[44] G. M. Sheldrick, SHELXTL PLUS, Göttingen and Siemens plc, **1990**.
[45] G. M. Sheldrick, SHELXL-93, Program for the refinement of crystal structures, University of Göttingen, Germany, **1993**.

0947-6539/98/0412-2592 $ 17.50+.50/0 *Chem. Eur. J.* **1998**, *4*, No. 12